Syntaxin 6 delays prion protein fibril formation and prolongs presence of toxic aggregation intermediates

Daljit Sangar, Kezia Jack, Mark Batchelor, Beenaben Mistry, Jan Bieschke*

MRC Prion Unit at UCL, Institute of Prion Diseases, Courtauld Building, London W1W 7FF, United Kingdom

*to whom correspondence should be addressed: j.bieschke@ucl.ac.uk

Abstract

Prions replicate via the autocatalytic conversion of cellular prion protein (PrP^C) into fibrillar assemblies of misfolded PrP. While this process has been extensively studied *in vivo* and *in vitro*, unphysiological reaction conditions of fibril formation *in vitro* have precluded the identification and mechanistic analysis of cellular proteins, which may alter PrP self-assembly and prion replication. Here, we have developed a fibril formation assay for recombinant murine and human PrP (23-231) under near-native conditions (NAA) to study the effect of cellular proteins, which may be risk factors or potential therapeutic targets in prion disease.

Genetic screening identified syntaxin 6 (Stx6) as a risk factor for Creutzfeldt-Jakob disease. Analysis of the protein in NAA revealed that Stx6 is a potent inhibitor of PrP fibril formation. It significantly delayed the lag phase of fibril formation at a highly sub-stoichiometric molar ratios. However, when assessing toxicity of different aggregation time points to primary neurons, Stx6 prolonged the presence of neurotoxic PrP species.

Electron microscopy and super-resolution fluorescence microscopy revealed that PrP formed less-ordered aggregates with Stx6 instead of highly ordered fibrils, which contained Stx6. These data strongly suggest that the protein directly alters PrP self-assembly and, uniquely, acts as an ‘anti-chaperone’, which promotes toxic aggregation intermediates by inhibiting fibril formation.

Introduction

Prion replication and prion-like mechanisms are believed to drive dozens of human neurodegenerative and systemic diseases as well as zoonoses, such as scrapie, bovine spongiform encephalopathy and chronic wasting disease (1-3). All of these disorders are caused by protein misfolding, but the details of the self-replication mechanism, the cellular factors involved in prion replication and the molecular basis for neurotoxicity are far from clear despite decades of research (4). Prions are fibrillar assemblies of misfolded cellular prion protein (PrP^C), which form highly ordered parallel in register intermolecular beta-sheet amyloid structures (prion rods, (5,6)). While purified prion rods are not directly neurotoxic, prion-associated toxicity can be blocked by anti-PrP antibodies (7,8) suggesting that non-fibrillar PrP assemblies could be the toxic agents, which form after prion titres plateau(9-11), as is the case for other amyloid forming proteins (12,13).

Prions can be highly infectious in zoonoses, however, accidental exposure only accounts for a tiny percentage of CJD cases. Similarly, mutations in the *PRNP* gene, which codes for the prion protein PrP, cause only 10-15% of CJD cases (14). It is likely that hidden genetic risk factors modulate either the susceptibility to prion replication or prion-associated neurotoxicity. A recent genome-wide association study to discover non-*PRNP* risk factors of CJD identified two highly significant risk loci for sCJD in or near to *STX6* (15). Elevated *STX6* mRNA in the caudate and putamen nuclei, two regions implicated in CJD pathology (16), correlated with CJD risk.

STX6 encodes syntaxin 6 (Stx6), an eight exon, 255 amino-acid protein that localises to the trans-Golgi network, and to recycling and early endosomes(17). Syntaxin 6 is thought to form part of the t-SNARE complex involved in the decision of a target membrane to accept the fusion of a vesicle (18). Misfolded prion protein in infected cells localizes at the plasma membrane, the likely site of prion conversion (19). Early and late endosomes, the endocytic recycling compartment and multivesicular bodies have also been implicated as prion replication sites (20,21). These observations raise two alternative mechanistic hypotheses for the role of syntaxin 6 in prion disease: (1) A direct interaction with PrP in the course of misfolding and prion replication, or (2) an indirect effect through the cellular processing of PrP^C or prions.

STX6 is a risk gene for progressive supranuclear palsy, where it interacts directly with tau through its transmembrane domain (22). Downregulation of syntaxin 6 expression in a murine neuroblastoma scrapie cell model (PK1) did not alter PrP^C expression and had no obvious effect on PrP^C trafficking (15), suggesting that it may directly alter prion replication by a yet undiscovered chaperone-like activity.

An array of chaperone proteins aid and tightly control protein folding and protein homeostasis in the cell (23,24). Chaperones, such as the heat shock protein Hsp70 inhibit protein misfolding and can delay amyloid formation *in vitro* (25) and in model organisms (26). It seems likely that more proteins with chaperone-like functions are yet to be discovered.

Assessing the role of proteins with chaperone-like activity in PrP misfolding, fibril formation and toxicity requires assays under native or near-native conditions. The established fibril formation assays for PrP *in vitro* require unphysiological conditions, such as high temperatures (27), denaturants (28), detergents or low pH (29). These conditions facilitate the unfolding and conversion of PrP^C, but preclude the analysis of other folded proteins in the context of PrP fibril formation. Here, we have developed a fibril formation assay for recombinant murine and human PrP^C (23-231) under near-native conditions to study the effect of syntaxin 6 and other cellular factors, which may be risk factors or potential therapeutic targets in prion disease.

Results

Full-length prion protein forms amyloid fibrils under near-native conditions

In order to study PrP fibril formation under near-native conditions *in vitro* full-length murine PrP^C 23-230 (mPrP23) and human PrP^C 23-231 (hPrP23) were expressed recombinantly (Figure S1), incubated in a non-binding 96-well plate under agitation with silanized zirconium beads, and amyloid formation was monitored via Thioflavin T (ThT) fluorescence (Figure 1, Figure S2). We tested different temperatures and pH values to assess whether PrP could form amyloid fibrils *in vitro* under near-native conditions (Figure S2A, B). While PrP was slow to form aggregates *de novo* without the addition of seeds, elevated temperatures accelerated fibril formation (Figure S2A) as had been previously observed (30). Aggregation at 42°C, pH 6.8 yielded highly reproducible conditions for the formation of fibrils (Figures 1C and S2B, C). Fibrils had diameters of 8-12 nm and morphologies typical of amyloid fibrils (Figures 2C and S2C). The addition of preformed fibrillar aggregates as seeds accelerated fibril formation in a concentration-dependent manner by decreasing lag-times (t_{50}, Figures 1A, B and S2D) but had no significant influence on rates of fibril elongation (Figure S2E). Lag phases and elongation rates of mPrP23 *in vitro* were indistinguishable when using synthetic seed formed from recombinant PrP^C or using authentic prion rods, isolated from mice infected with scrapie strains RML or ME7 in (Figures S2D, E and S3). Interestingly, fibrils formed from synthetic seeds displayed increased ThT fluorescence when compared to RML and ME7 seeded fibrils, hinting at a difference in fibril structure imprinted by the different seed templates (Figure 1F). For safety reasons, seeding of hPrP23 was restricted to synthetic PrP fibrils.

The lag phase of hPrP23 aggregation depended only weakly on PrP monomer concentration (Figure 1D, E), while elongation rates even showed a slight inverse reaction to monomer concentration (Figure 1F). Therefore, PrP refolding may be rate-limiting under the assay conditions. ThT amplitude at the end of growth was proportional to monomer concentration (Figure 1G). However, the lag phase increased and ThT amplitude dropped at monomer concentrations above 16 µM, suggesting formation of off-pathway PrP aggregates at high monomer concentrations, which do not contribute to fibril formation (31).

Syntaxin 6 inhibits PrP fibril formation

The STX6 gene is a known risk factor for Creutzfeldt-Jacob disease, suggesting it may alter PrP fibril formation. We therefore tested what effect the syntaxin 6 protein (Stx6) had on PrP fibril formation and compared it to heat shock protein Hspa1a, which a the human inducible

form of Hsp70, and the α-helical microtubule-associated protein Stathmin 1 (Stmn1) as controls (Figure S1A). Circular dichroism confirmed that Stx6 retained its native α-helical fold under assay conditions (Figure S1B).
To our surprise, Stx6 delayed the lag phase of hPrP23 fibril formation even at highly sub-stoichiometric molar ratios of 1:100, and prevented fibril formation entirely at equimolar ratio (Figure 2A, B). At the same time, it slightly lowered fibril elongation rates (Figure 2C). Syntaxin promoted the formation of aggregate with a more amorphous morphology, which seemed to consist of clusters of short fibrils (Figure 2D, E). Immuno-gold staining revealed that syntaxin 6 was incorporated into these aggregates (Figure 2F). Similarly, Hspa1a prevented fibril formation in favour of amorphous PrP aggregates, which incorporated the chaperone (Figure S4), while hPrP23 formed fibrillar aggregates in the presence of control protein Stmn1.

To further probe the interaction of Stx6 with PrP aggregates and fibrils we used dSTORM and TAB super-resolution microscopy (Figures 3 and S5). When monomeric hPrP23 and Stx6 were co-incubated at 1 : 0.1 molar ratio, they co-aggregated into assemblies with amorphous morphology (Figure S5). Super-resolution microscopy indicated a fibrillar substructure of these aggregates similar to that observed in TEM (Figure 2E). However, when Stx6 labelled with AlexaFluor647 was added to pre-formed fibrillar hPrP23, it preferentially bound to specific ‘hot-spots’ on the PrP fibril (Figure 3A, B, indicated by arrows). We repeated the experiment with Stx6-AlexaFluor488 (Figure 3E) to exclude that the interaction was influenced by the choice of fluorescent dye, which confirmed the presence of interaction hot-spots. In both cases, hPrP23 fibrils were unlabelled and were visualized by TAB imaging using the amyloidophilic dye Nile red (32). Interestingly, interaction sites were often located at fibril ends or kinks in the fibril. Since Stx6 only weakly affected apparent fibril elongation rates in bulk assays, this may suggest a role of Stx6 in fibril breakage or secondary nucleation.

Inhibition of PrP fibril formation depends on salt concentration

To further probe the mechanism of Stx6, we tested the influence of NaCl concentration on fibril formation in the presence and absence of Stx6 (1:0.1 molar ratio) and compared kinetics in the presence of Stx6 to those in the presence of Hspa1a and Stmn1, respectively, at the same molar ratio (Figure 4A). HspA1A delayed fibril formation to a similar degree as Stx6, while Stmn1 had no significant effect on fibril formation kinetics. In the absence of Stx6, the lag phase of PrP fibril formation decreases only weakly with NaCl concentration while the elongation rate increased (Figure 4B, C). Syntaxin 6 prolonged the lag phase at

low and physiological salt concentrations, but lag phases decreased with increasing NaCl concentration, indicating that ionic interactions mediate the binding of Stx6 to PrP. A similar salt dependence was observed for HspA1A (Figure 4D), while Stmn1 did not inhibit fibril formation at any salt concentration (Figure 4E). Stx6 did not significantly reduce fibril elongation when compared with untreated PrP independently of salt concentration (Figure 4C).

Syntaxin 6 prolongs the presence of toxic PrP aggregation intermediates

All of the previous data would suggest a protective rather than deleterious effect of syntaxin 6 in prion disease. However, the oligomer toxicity hypothesis posits that mature fibrils may not be the toxic species in prion nor in other amyloid diseases (11,12). Correspondingly, purified, highly infectious prion rods were not toxic to primary neurons (7). To test whether the same logic applied to the effect of Stx6 on PrP aggregation, we assessed the toxicity of PrP to mouse primary neurons at different stages of the aggregation kinetics (Figure 5). PrP aggregates were highly toxic to primary neurons during lag and early growth phases (20h and 40h incubation), but neurotoxicity was diminished at the plateau phase of fibril formation, so that end-point aggregates (90h) were no more toxic than PrP monomers or buffer controls (Figure 5 A, C).

In contrast, PrP aggregated in the presence of Stx6 (1:0.1 molar ratio) retained its neurotoxicity significantly longer than PrP incubated in the absence of Stx6 (Figure 5B, C). While PrP species formed early in the lag phase of aggregation at 20h were neurotoxic both in the presence and absence of Stx6 when compared to t = 0h, PrP was significantly more toxic in the presence of Stx6 at later time-points when PrP would form fibrils in the absence of Stx6 (Figure 6C). Thus, in delaying or preventing PrP fibril formation, Stx6 prolonged the presence of toxic aggregation intermediates and exacerbated neurotoxicity.

Discussion

Native aggregation assay

We developed a fibril formation assay for full length mouse and human PrP^C to be able to study the mechanistic effect of cellular proteins such as the CJD risk factor syntaxin 6 on PrP misfolding and self-assembly under near-native conditions. A multitude of *in vitro* fibril formation assays have been developed (33). While the generation of authentic prion infectivity was reported for several assays (28,33), fibrils generally form under highly

unphysiological conditions in the presence of high concentrations of Guanidine or Urea (28), at low pH (34), in the presence of SDS (35), or at very high temperatures (36). None of these condition provide a native environment for protein-protein interaction, and many cellular proteins will be unfolded under the assay conditions.

Full length PrP formed fibrils with morphology and β-sheet secondary structure, which are typical for amyloid, under conditions of our native aggregation assay (NAA) (37). Fibril formation could be tracked by binding of the amyloidophilic dye Thioflavin T and displayed sigmoid aggregation kinetics typical of a nucleated polymerization mechanism (38). As had been observed for other amyloidogenic proteins, solution conditions such as pH and temperature affected aggregation kinetics (39,40). Aggregation proceeded faster at neutral pH, while monomeric protein was stable at pH of 6.5 and below.

Seeding by preformed fibrils reduced the lag phase of aggregation (41,42). The limiting dilution for seeding was ~ 10^{-10} (w/w), which corresponds to approximately 2000 PrP molecules per well or 5 prion rods of a typical length of 200 nm (43), similar to other seeding assays (35,36,44). In NAA, both lag phase t_{50} and elongation rate constant k displayed little dependence on monomer concentration, which suggests that monomer refolding was rate limiting for fibril elongation. While generally, aggregation kinetics scale with monomer concentration, elongation saturates at high monomer concentration as conformational change of PrP becomes rate-limiting (45,46). ThT fluorescence amplitudes scaled with PrP concentration between 2 – 16 µM, it then dropped and lag phase increased. A competing non-fibrillar aggregation pathway at high protein concentration could account for this observation (31,47). High salt concentration shields charges, which promotes hydrophobic interactions, lowers the critical concentration of nucleated polymerization often leading to formation of amyloid fibril clusters (48). Notably, while PrP aggregated faster in the NAA at high salt concentration, it tended to form longer, more isolated fibrils.

Inhibition by syntaxin 6

Syntaxin 6 delayed the formation of PrP fibrils at highly sub-stoichiometric ratios and co-aggregated with PrP into amorphous assemblies similar to the effect of heat shock protein family A (Hsp70) member 1A (Figures 2 and 4). On the face, this would suggest a role of Stx6 as a potent aggregation inhibitor with chaperone-like activity. Chaperones assist folding of newly synthesised proteins, sequester soluble misfolded polypeptides and target them for degradation, which makes them promising therapeutic targets in protein misfolding diseases (24,49,50).

Hsp70 has been described as a ‘holdase’, which inhibits amyloid formation of various proteins at substoichiometric concentrations even in the absence of ATP by binding to early stage aggregation intermediates (51,52). Overexpression or exogeneous addition of Hsp70 rescued cytotoxicity in cell cultures and model organisms (53-55). Sequestering aggregation intermediates into inert off-pathway aggregates can be a powerful strategy against amyloid toxicity (56,57). However, our data indicate that, far from detoxifying PrP aggregation intermediates, the redirection of PrP fibrils into amorphous aggregates by Stx6 exacerbated PrP toxicity by allowing toxic aggregation intermediates to persist for longer (Figure 5).

Conversely, natural and chemical chaperones can detoxify aggregation intermediates by promoting fibril formation and by stabilizing mature amyloid fibrils (42,58,59). Syntaxin 6 seems to present the flip side of this benign activity in delaying PrP fibril formation and thus prolonging the presence of toxic aggregation intermediates.

The nature of the toxic species in prion disease is under active investigation. Brain homogenates from scrapie-infected mice have a specific toxic component, which can be blocked by the addition of anti-PrP antibody (7). However, highly purified infectious prion rods were not directly neurotoxic (7), suggesting that toxicity may be caused by non-prion assemblies, which accumulate after the infectious titer has peaked and which, unlike prions, are sensitive to salkosyl (8-10) or by transient aggregation intermediates, whose formation may be catalysed by prions or by other fibrillar PrP assemblies (4).

The chaperone Brichos breaks generation of toxic Aβ oligomers, which are formed through surface catalysed secondary nucleation (60). Conceivably, syntaxin 6 could have the opposite effect on PrP fibril formation, in which toxic oligomer formation is promoted, by delaying competing fibril formation pathways. PrP itself binds to and inhibits the elongation of Abeta amyloid fibrils (61,62) oligomers and nanotubes. The presence of PrP during aggregation led to the formation of larger numbers of shorter fibrils and increased Aβ neurotoxicity in a dose-dependent manner (61). This suggests that PrP not only acts as a receptor for toxic amyloid oligomers (63,64), but exacerbates neurotoxicity in a mechanism similar to Stx6. Notably, Stx6, when added to preformed fibrils, preferentially bound to fibril ends and other hotspots (Figure 3). Previous studies found weak binding of Stx6 to monomeric PrP^C (15), which together with the inhibition at sub-stoichiometric concentrations strongly suggests an interaction with fibrillary assemblies and with early aggregation intermediates. Inhibition was suppressed by high salt concentration, indicating a charge-mediated interaction between Stx6 and PrP (Figure 4).

Localization of syntaxin 6 and PrP

A direct effect of syntaxin 6 on prion replication and / or prion-associated toxicity *in vivo* obviously requires the two proteins to be present in the same sub-cellular compartment. PrP^C is present mainly in the Trans Golgi Network and on the outer plasma membrane, mature PrP^C is tethered to the membrane by a C-terminal glycophosphadityl-inositol (GPI) anchor. At the plasma membrane, PrP^C is incorporated into lipid rafts and caveolae, which are membrane microdomains enriched in cholesterol and sphingolipids. However, it has also been detected in multi-vesicular bodies and, to a small degree, in the cytosol (65). Both lipid rafts and the endocytic pathway are implicated as sites of prion replication (65).

Interestingly, Stx6 has role in caveolin membrane recycling (66). As a SNARE protein, Stx6 sits on the outside of vesicles and on the inner plasma membrane, so that a direct interaction with PrP would require mislocation of either protein. Both, PrP and syntaxin 6 contain a trans-membrane domain and PrP can populate transmembrane forms in neurons (67,68). It is therefore plausible that, similar to the tau protein, PrP and prions bound to the membrane bilayer could interact with the transmembrane domain of syntaxin 6. Alternatively, mislocation of misfolded PrP assemblies could facilitate interaction with Stx6. Amyloid assemblies can disrupt membrane integrity through mechanical rupture, pore formation or altering membrane curvature (69,70). Disruption of membranes on the cell surface and in vesicles of the endocytic pathway, is a central step in the internalization of other misfolded polypeptides, such as Amyloid-β (71,72). Similarly, it has been hypothesized to be necessary for cellular prion propagation (21). These processes could bring misfolded PrP into direct contact with syntaxin 6.

Conclusions

We developed aggregation assay of murine and human prion protein under near-native conditions. PrP forms amyloid fibrils under assay conditions, which bypass primary nucleation through seeding and accelerate fibril formation when compared to the unseeded reaction. Unlike natively unfolded proteins, however, PrP fibril formation does not scale strongly with monomer and seed concentrations, suggesting that structural conversion of native PrP into the amyloid fold is rate limiting. This is consistent with the observation that the time constant of exponential prion replication *in vivo* is independent of PrP expression (9).

In the NAA both the PrP and potential protein modulators of aggregation are in their native conformation, which means that mechanisms by which protein and small modulators alter amyloid formation can be assessed. We analyzed the effect of syntaxin 6, a recently discovered risk factor for CJD, on PrP self-assembly. To our surprise, we discovered the

protein to act as an ‘anti-chaperone’, which, by delaying PrP fibril formation, prolonged the persistence of toxic aggregation intermediates *in vitro*.

While at this point we cannot assess whether the toxicity of PrP aggregation intermediates formed *in vitro* recapitulates the authentic PrP species responsible for neurotoxicity in prion disease *in vivo*, our data highlight a new mechanism by which protein modulators of amyloid formation can have counter-intuitive deleterious effects.

Acknowledgements

Research was supported by the National Institute of Neurological Disorders and Stroke of the National Institutes of Health grant number 1R21NS101588-01A1 and by MRC grant MC_UU_00024/6 to JB. We thank Adam Wenborn and Dr. Jonathan Wadsworth, MRC Prion Unit, for providing mouse scrapie material and mass spectrometry and Prof. Erich Wanker, MDC-Berlin, Germany for providing E. coli clones for protein expression.

Methods and Materials

Protein Expression and Purification:

Human PrP (23-231), Mouse PrP (23-231)

The open reading frame of the human PrP gene (PRNP) (residues 23-231), containing methionine at residue 129 and the mouse PrP gene (Prnp) (residues 23-231), was synthesised de novo by Eurofins MWG Operon, with a thrombin-cleavable His-Tag added to the PrP N-terminus. The ligated pTrcHisB/PRNP and pTrcHisB/Prnp constructs were used to transform the Escherichia coli host strain BL21(DE3) (Novagen), genotype F′ ompT hsdSB (rB- mB-) gal dcm (DE3), which was then plated onto Luria-Bertoni (LB) agar plates containing 100 µg / mL carbenicillin. Cultures were grown for purification using a modification of protocols previously described (73). Briefly, following harvesting, cells were sonicated and their inclusion bodies containing PrP resolubilised in 6 M Guanidine Hydrochloride (GuHCl), 50 mM Tris-HCl, 0.8% β-mercaptoethanol, pH 8.0. These were loaded onto a Ni-NTA column equilibrated in 6 M GuHCl, 10 mM Tris-HCl, 100 mM Na_2PO_4, 10 mM glutathione pH 8.0, and eluted from the column using 10 mM Tris-HCl, 100 mM Na_2PO_4, 2 M Imidazole pH 5.8. Residual GuHCl was removed through dialysis against 20 mM Bis Tris.HCl pH 6.5, $CaCl_2$ added to a final concentration of 2.5 mM, and the N-terminal His-tag cleaved by thrombin for 16 h at room temperature (0.1 U thrombin (*Novagene*) / 1 mg of PrP added). The cleaved protein was loaded onto a second Ni NTA column equilibrated with 20 mM Bis-Tris pH 6.5, 25 mM imidazole pH 6.5 and the PrP eluted by the same buffer containing 2 M imidazole pH 6.5. Peak containing the purified PrP^{231} was collected and dialysed against 10 mM Bis Tris pH 6.5, and aliquoted and stored at -80ºC. Protein concentrations were determined by UV absorption at 280 nm using a calculated molar extinction of 56667 M^{-1} cm^{-1} and 57995 M^{-1} cm^{-1} for human and mouse PrP, respectively (*https://web.expasy.org/protparam*).

SEC of Syntaxin 6 / Human Prp (23-231) / Mouse Prp (23-231)

2 mL Pre-concentrated, pre-cleared protein was loaded via injection valve onto a Sephacryl S100HR column (GE Healthcare) (26/60 : 320 mL bed volume) that had been pre-equilibrated with 20 mM Tris-HCl, 0.2 M NaCl, pH 8. A flow-rate of 2 mL / min was used; all eluted peaks were checked on a silver stained NuPage Bis Tris 12% gel, using the protocol according to the silver staining kit (SilverQuest Silver Staining Kit-1, LC6070, Life Technologies Ltd) and the purified protein was aliquoted and stored at −80°C until use.

Stathmin 1 (STMN1) / Heat-Shock Protein 70 (HSPA1A)

Glycerol stocks of E. Coli BL21 strains expressing His-tagged Stmn1 and Hspa1a were a gift by E. Wanker, MDC-Berlin, Germany. Small scale cultures of STMN1 and Hspa1a were cultured in LB/Amp (100 µg / mL) by inoculating with stabs from glycerol stocks. Cells were pelleted and then inclusion bodies lysed in 1 mL lysis buffer (containing 50 mM Tris, 0.2M NaCl, pH8 containing 0.1% Tween20, 0.5% NP40, 50 U/mL Benzonase, 10 µg / mL Lysozyme and 1mM PMSF) placed on ice for 1 h with gentle vortexing every 15 min. (All centrifugations were done at 4°C to further prevent non-specific cleavage by proteases and samples were kept on ice.) The lysate was cleared by centrifugation (1h, 16100rpm) and then loaded onto 2 mL NiNTA resin bed packed in mini spin columns, pre-equilibrated with buffer containing 50mM NaH_2PO_4, 0.3 M NaCl, 20 mM Imidazole at pH 8. The cleared lysate was loaded onto the column, unbound was eluted off the column first with gentle centrifugation (2 min 2000 rpm); the resin was washed to thoroughly remove unbound protein by twice loading 700 µl pre-equilibration buffer (see above) and centrifugation for 30 s, 2000rpm and then 2 min, 2000rpm for the second wash. Finally, the pure protein was eluted in elution buffer (containing 50 mM NaH_2PO_4, 0.5 M NaCl, 0.5 M imidazole, pH 8). This was done by loading 100 µl elution buffer with a 30 s centrifugation at 2000 rpm followed by a second elution with 150 µl elution buffer and a 2 min centrifugation at 2000 rpm. Both fractions were pooled and checked for purity as below.

The purified STMN1 and Hsp70 recombinant proteins were checked for purity by coomassie staining after PAGE on NuPage BisTris 12% gels. Protein identity was confirmed by mass spectrometry following a standard trypsinization protocol on a Waters Xevo-XS spectrometer as described in (5).

Syntaxin 6 (STX6)

Syntaxin-6 (residues 38-318; Accession number KU144824) was prepared according to (74) with modifications. Briefly, the DNA sequences encoding the syntaxin-6 protein in pQTEV were transformed into BL21 (DE3). BL21 cultures were grown in LB medium in the presence of 100 µg / mL Ampicillin. Expression of the protein was induced using 1 mM IPTG and was purified from inclusion bodies under denaturing conditions using Nickel superflow resin with an AKTA Pure (GE health care Life Sciences). The protein was eluted from the column using

an imidazole gradient. The eluted material was extensively dialysed against 20 mM Tris, 2 mM EDTA, 10 mM DTT, 200 mM NaCl pH 8.0. Stx6 was further purified by size exclusion chromatography on a Sephacryl S100HR column (GE Healthcare) (26/60: 320 mL bed volume) in 20 mM Tris buffer, 0.2 M NaCl, pH 8. The final concentration of the syntaxin-6 protein was determined by absorption measurement at 280 nm, ε = 31970/M/cm. Aliquots were stored at −80°C until use.

Circular Dichroism (CD) spectroscopy

CD data were recorded on a Jasco J-715 spectrophotometer equipped with a thermoelectric temperature controller. A 1 mm path length cuvette was used for all CD spectroscopy measurements. Wavelength measurements were recorded from 190 nm to 260 nm at 20ºC, using 0.36 mg / mL syntaxin-6 in 10 mM Na-phosphate, pH 8.

Native Aggregation Assay (NAA)

PrP^C was filtered through a 100kD membrane filter in 10 mM Bis Tris pH 6.5 (Amicon ULTRA 0.5 mL 100K 96PK, UFC510096, Merck Life Science UK Ltd) to remove large aggregates and then diluted into reaction buffer (50mM Na-phosphate, pH 6.8, 150 mM NaCl, 0.01% Na-Azide, 20 µM ThT and 5 mM Bis-Tris pH 6.5) with the addition of 0.1% seed (w/w), unless indicated otherwise. The standard final concentrations of PrP and NaCl were 2.5 µM and 150 mM, pH 6.8 unless indicated otherwise. The seed consisted of aggregated PrP material from an unseeded reaction under the same conditions as above. It was diluted to 10% (w/w) in 5 mM Bis-Tris, pH 6.5 and sonicated in a water bath sonicator (GRANT, XUBA1) for 15 min prior to addition to the reaction mix. Aggregation assays for neuronal toxicity were set up in parallel to the standard assays for kinetic analysis, but here the ThT and Na-Azide was omitted from the reaction mixes.

The seed and post aggregation samples were handled with pre-silanised tips, in pre-silanised non-binding tubes (Repel-silane ES, Sigma, 17-1332-01). The reaction mix (94 µl per well) was dispensed into low binding 96 well COSTAR (#3651) plates and three silanised zirconium beads (0.5 mm diameter, Figures 1-4 and S2-S7; 1 mm diameter, Figure 5) were added to each well. ThT kinetics were recorded on a BMG ClarioStar plate reader at 42°C with a shaking speed of 700 rpm, set to shake for 100 s with an incubation time of 20 s between

agitation. Focal height was set to 20 mm, top read, with excitation at 440 nm and emission set to 485 nm.

EM grid preparation

End-point samples (5-6 µL) from native aggregation assays sonicated in a water bath for 10-15 s were loaded onto carbon-coated 300 mesh copper grids (Electron microscopy Sciences) that had been glow discharged for 40 seconds using an PELCO easiGLOW™ glow discharge unit (Ted Pella Inc., USA). Samples were left to bind for 30 min, blotted dry, washed in water (1 x 50 µL), blotted, and then stained with 10 µL Nano-W (methylamine tungstate) stain (Nanoprobes) for 1 min followed by 30 s (with blotting in between stain times). Images were acquired on a Talos electron microscope (FEI, Eindhoven, NL now ThermoFisher).

Immunolabelling EM grids

6 µL endpoint aggregation sample was allowed to adsorb to surface of glow discharged grids for 60 min post 10 s sonication in a water bath sonicator (GRANT, XUBA1). Excess liquid was removed by touching edge of grid on filter paper. Grids were blocked with 50 µl 2% BSA in TBS containing 0.1% sarkosyl followed by quick sequential washing/blotting steps in 5x 50 µl drops of TBS containing 0.1% sarkosyl followed by 1 h incubation with primary antibody diluted (1:100) in TBS containing 0.1% sarkosyl. After a second round of washing/blotting steps with 5x 50 µl drops of TBS containing 0.1% sarkosyl, the grid was incubated with secondary antibody which was diluted (1:20) in TBS containing 5% (v/v) glycerol. The final wash step was done with sequential washing / blotting in 3 x TBS and then grid stained with 10 µL Nano-W (methylamine tungstate) stain (Nanoprobes) for 1 min followed by 30 s blotting in between stains.

To preserve the carbon coating on the surface of the grid, the antibody incubations and blocking / washing steps were carried out by placing the grid sample side down on top of a 50 µL drop of the dilute antibody or buffer, momentarily for TBS washes, or for 1 h per antibody and blocking step.

For detection of STX6 labelled species, the primary Ab used was Syntaxin 6 (C34B2) Rabbit mAb 2869 (Cell Signaling Technology Europe B.V, 2869S).

For detection of STMN1 labelled species, the primary Ab used was Stathmin 1 Rabbit Polyclonal Antibody (Insight Biotechnology Ltd, GTX104707).

For detection of Hsp70 (HSPA1A) labelled species, the primary antibody used was Hsp70 Rabbit Polyclonal Antibody (Insight Biotechnology Ltd, 10995-1-AP).

The secondary antibody used for all samples was Goat anti-Rabbit IgG conjugated to colloidal gold (10 nm) (Insight Biotechnology Ltd, GA1014).

SR sample preparation

8-well chamber slides (IBL Baustoff, 2 20.140.082, C8-1.5-H-N, 8 well chambered cover glass with #1.5 high performance cover glass, 0.170 +/- 0.005 mm) were cleaned by soaking them overnight in a 2% solution of Hellmanex II detergent diluted in ultrapure water and then washed thoroughly in ultrapure water before rinsing in 100% methanol and then a final thorough rinse in ultrapure water and then allowing the slides to dry.

Once dry, the slides were glow discharged for 40 seconds using an PELCO easiGLOW™ glow discharge unit (Ted Pella Inc., USA). 10 µL sample was added to the centre of a well and allowed to incubate for 1 h for the fibrils to adhere to the glass. The well was then washed 5X with 500 µL of HPLC purified water before 200 µL buffer (which consists of 50 nM Nile Red (Sigma-Aldrich, 72485-1G in PBS or GLOX buffer). The wells are then sealed either with Nescofilm or TWINSIL before imaging on a custom built TAB/dSTROM super-resolution microscope (75).

Enzymatic oxygen scavenger (GLOX, glucose oxidase with catalase) buffer consisted of two solutions. Solution A: Tris (50 mM, pH 8.3), NaCl (10 mM), glucose (10% w/v), and β-mercaptoethylamine (Sigma-Aldrich, 30070, 10 mM). Solution B: glucose oxidase (Sigma-Aldrich, G2133, 8 mg), and catalase (Sigma-Aldrich, C100, 38 µL, 21 mg / mL) in PBS (160 µL). Solutions A and B were mixed at the ratio of 99:1 (v/v) immediately before use.

Labelling recombinant protein with AlexaFluor dyes

AlexaFluor Dyes (Alexa Fluor™ 647 C2 Maleimide, A20347, Alexa Fluor™ 488 C5 Maleimide, A10254, thermofisher.com) were diluted in DMSO to a stock concentration of 10 mg / mL. The dyes were mixed with the recombinant protein constructs at a molar ratio of 2:1 dye:protein construct. The mixture of dye and protein constructs were protected from light by covering the vessel with foil and left to mix on a rotator overnight at 4°C. The following day, the unbound dye was removed by dialysis in 2.5 l for 2 x 1 h, in a suitable buffer with 8 kD dialysis membrane (SpectraPor 7 8000 Dalton MWCO; 11425919, Fisher Scientific UK). For Stx6 the buffer used for dialysis was 10 mM Na-phosphate,150 mM NaCl, 2 mM EDTA, 2 mM DTT, pH 8; for PrP,

the buffer used for dialysis was 10 mM Bis-Tris, pH 6.5. Once dialysis was complete, the labelled protein was recovered from the dialysis membrane and checked on a 4-12% Bis-Tris gel. To check labelling efficiency, an absorption spectrum measurement (200-700 nm) was taken and the final concentrations of dye and protein were calculated according to the manufacturer protocol. The labelled proteins were then aliquoted and stored at -80°C.

Primary Neuronal Culture and Toxicity Analysis

Primary neuronal cultures were derived from brains of inbred FVB/N mice. Hippocampi of E17 mouse brains were dissected in HBSS (ThermoFisher Scientific) supplemented with 1% L-glutamine, 1% HEPES and 1% pen-strep. Cells were dissociated using 0.25% trypsin+0.04% benzonase, triturated mechanically and counted using a Neubauer haemocytometer. Cells were plated in DMEM supplemented with 10% horse serum (#26050-88, Invitrogen) at 10K/well to the inner 60 wells of poly-L-lysine- coated 96 well plates (Greiner, 655936). At 1 h post-plating, DMEM medium was aspirated and exchanged for Neuralbasal medium (21103049, ThermoFisher Scientific) supplemented with 0.25% Glutamax (35050061, ThermoFisher Scientific) 2% Gibco B27 supplement (17504044, ThermoFisher Scientific) and incubated at 37°C (20% O2, 5% CO2). FVB/N neurons were maintained in culture for 11-12 days prior to a 96 h treatment. Images of live cells were taken on an IncuCyte S3 reader (Sartorius) with a 20x objective in phase contrast. 4 views were captured in each well every 4 h. PrP samples were diluted 1:10 into fresh media and added at the 24 h mark.

Neurite lengths were evaluated using the NeuroTrack module of the IncuCyte S3 software package (rev 2019A) using the following parameters: cell body cluster segmentation 0.7; cleanup 0; cluster filter 0; neurite sensitivity 0.25; neurite width 1 µm. Detected neurite masks are highlighted in pink in images. Neurite length data were normalized to the initial (0 h) value for each well and means ± standard deviation were calculated from quintuplicate sample wells. Average neurite lengths at the 80-100 h time interval were visualized in a box plot and ANOVA statistical analysis (two-tailed, equal variances) was performed in OriginPro 2019.

Work with animals was performed under the licence granted by the UK Home Office (Project Licences 70/6454 and 70/7274) and conformed to University College London institutional and ARRIVE guidelines.

References

1. Prusiner, S. B. (1998) Prions. *Proc Natl Acad Sci U S A* **95**, 13363-13383
2. Brundin, P., Melki, R., and Kopito, R. (2010) Prion-like transmission of protein aggregates in neurodegenerative diseases. *Nat Rev Mol Cell Biol* **11**, 301-307
3. Frost, B., and Diamond, M. I. (2010) Prion-like mechanisms in neurodegenerative diseases. *Nat Rev Neurosci* **11**, 155-159
4. Collinge, J., and Clarke, A. R. (2007) A general model of prion strains and their pathogenicity. *Science* **318**, 930-936
5. Manka, S. (2022) 2.7 Å cryo-EM structure of ex vivo RML prion fibrils. *Nature Communications* **13**
6. Kraus, A., Hoyt, F., Schwartz, C. L., Hansen, B., Artikis, E., Hughson, A. G., Raymond, G. J., Race, B., Baron, G. S., and Caughey, B. (2021) High-resolution structure and strain comparison of infectious mammalian prions. *Mol Cell* **81**, 4540-4551 e4546
7. Benilova, I., Reilly, M., Terry, C., Wenborn, A., Schmidt, C., Marinho, A. T., Risse, E., Al-Doujaily, H., Wiggins De Oliveira, M., Sandberg, M. K., Wadsworth, J. D. F., Jat, P. S., and Collinge, J. (2020) Highly infectious prions are not directly neurotoxic. *Proc Natl Acad Sci U S A* **117**, 23815-23822
8. Reilly, M., Benilova, I., Khalili-Shirazi, A., Schmidt, C., Ahmed, P., Yip, D., Jat, P. S., and Collinge, J. (2022) A high-content neuron imaging assay demonstrates inhibition of prion disease-associated neurotoxicity by an anti-prion protein antibody. *Sci Rep* **12**, 9493
9. Sandberg, M. K., Al-Doujaily, H., Sharps, B., Clarke, A. R., and Collinge, J. (2011) Prion propagation and toxicity in vivo occur in two distinct mechanistic phases. *Nature* **470**, 540-542
10. Sandberg, M. K., Al-Doujaily, H., Sharps, B., De Oliveira, M. W., Schmidt, C., Richard-Londt, A., Lyall, S., Linehan, J. M., Brandner, S., Wadsworth, J. D., Clarke, A. R., and Collinge, J. (2014) Prion neuropathology follows the accumulation of alternate prion protein isoforms after infective titre has peaked. *Nat Commun* **5**, 4347
11. Collinge, J. (2016) Mammalian prions and their wider relevance in neurodegenerative diseases. *Nature* **539**, 217-226
12. Haass, C., and Selkoe, D. J. (2007) Soluble protein oligomers in neurodegeneration: lessons from the Alzheimer's amyloid beta-peptide. *Nat Rev Mol Cell Biol* **8**, 101-112
13. Corbett, G. T., Wang, Z., Hong, W., Colom-Cadena, M., Rose, J., Liao, M., Asfaw, A., Hall, T. C., Ding, L., DeSousa, A., Frosch, M. P., Collinge, J., Harris, D. A., Perkinton, M. S., Spires-Jones, T. L., Young-Pearse, T. L., Billinton, A., and Walsh, D. M. (2020) PrP is a central player in toxicity mediated by soluble aggregates of neurodegeneration-causing proteins. *Acta Neuropathol* **139**, 503-526
14. Mead, S., Lloyd, S., and Collinge, J. (2019) Genetic Factors in Mammalian Prion Diseases. *Annu Rev Genet* **53**, 117-147
15. Jones, E., Hummerich, H., Vire, E., Uphill, J., Dimitriadis, A., Speedy, H., Campbell, T., Norsworthy, P., Quinn, L., Whitfield, J., Linehan, J., Jaunmuktane, Z., Brandner, S., Jat, P., Nihat, A., How Mok, T., Ahmed, P., Collins, S., Stehmann, C., Sarros, S., Kovacs, G. G., Geschwind, M. D., Golubjatnikov, A., Frontzek, K., Budka, H., Aguzzi, A., Karamujic-Comic, H., van der Lee, S. J., Ibrahim-Verbaas, C. A., van Duijn, C. M., Sikorska, B., Golanska, E., Liberski, P. P., Calero, M., Calero, O., Sanchez-Juan, P., Salas, A., Martinon-Torres, F., Bouaziz-Amar, E., Haik, S., Laplanche, J. L., Brandel, J. P., Amouyel, P., Lambert, J. C., Parchi, P., Bartoletti-Stella, A., Capellari, S., Poleggi, A., Ladogana, A., Pocchiari, M., Aneli, S., Matullo, G., Knight, R., Zafar, S., Zerr, I., Booth, S., Coulthart, M. B., Jansen, G. H., Glisic, K., Blevins, J., Gambetti, P., Safar, J., Appleby, B., Collinge, J., and Mead, S. (2020) Identification of novel risk loci and

causal insights for sporadic Creutzfeldt-Jakob disease: a genome-wide association study. *Lancet Neurol* **19**, 840-848
16. Meissner, B., Kallenberg, K., Sanchez-Juan, P., Ramljak, S., Krasnianski, A., Heinemann, U., Eigenbrod, S., Gelpi, E., Barsic, B., Kretzschmar, H. A., Schulz-Schaeffer, W. J., Knauth, M., and Zerr, I. (2009) MRI and clinical syndrome in dura mater-related Creutzfeldt-Jakob disease. *J Neurol* **256**, 355-363
17. Jung, J. J., Inamdar, S. M., Tiwari, A., and Choudhury, A. (2012) Regulation of intracellular membrane trafficking and cell dynamics by syntaxin-6. *Biosci Rep* **32**, 383-391
18. Wendler, F., and Tooze, S. (2001) Syntaxin 6: the promiscuous behaviour of a SNARE protein. *Traffic* **2**, 606-611
19. Goold, R., Rabbanian, S., Sutton, L., Andre, R., Arora, P., Moonga, J., Clarke, A. R., Schiavo, G., Jat, P., Collinge, J., and Tabrizi, S. J. (2011) Rapid cell-surface prion protein conversion revealed using a novel cell system. *Nat Commun* **2**, 281
20. Yamasaki, T., Suzuki, A., Hasebe, R., and Horiuchi, M. (2018) Retrograde Transport by Clathrin-Coated Vesicles is Involved in Intracellular Transport of PrP(Sc) in Persistently Prion-Infected Cells. *Sci Rep* **8**, 12241
21. Yim, Y. I., Park, B. C., Yadavalli, R., Zhao, X., Eisenberg, E., and Greene, L. E. (2015) The multivesicular body is the major internal site of prion conversion. *J Cell Sci* **128**, 1434-1443
22. Lee, W. S., Tan, D. C., Deng, Y., van Hummel, A., Ippati, S., Stevens, C., Carmona-Mora, P., Ariawan, D., Hou, L., Stefen, H., Tomanic, T., Bi, M., Tomasetig, F., Martin, A., Fath, T., Palmer, S., Ke, Y. D., and Ittner, L. M. (2021) Syntaxins 6 and 8 facilitate tau into secretory pathways. *Biochem J* **478**, 1471-1484
23. Hartl, F. U. (2011) Chaperone-assisted protein folding: the path to discovery from a personal perspective. *Nat Med* **17**, 1206-1210
24. Balch, W. E., Morimoto, R. I., Dillin, A., and Kelly, J. W. (2008) Adapting proteostasis for disease intervention. *Science* **319**, 916-919
25. Glover, J. R., and Lindquist, S. (1998) Hsp104, Hsp70, and Hsp40: a novel chaperone system that rescues previously aggregated proteins. *Cell* **94**, 73-82
26. Thackray, A. M., Lam, B., McNulty, E. E., Nalls, A. V., Mathiason, C. K., Magadi, S. S., Jackson, W. S., Andreoletti, O., Marrero-Winkens, C., Schatzl, H., and Bujdoso, R. (2022) Clearance of variant Creutzfeldt-Jakob disease prions in vivo by the Hsp70 disaggregase system. *Brain*
27. Atarashi, R., Sano, K., Satoh, K., and Nishida, N. (2011) Real-time quaking-induced conversion: a highly sensitive assay for prion detection. *Prion* **5**, 150-153
28. Legname, G., Baskakov, I. V., Nguyen, H. O., Riesner, D., Cohen, F. E., DeArmond, S. J., and Prusiner, S. B. (2004) Synthetic mammalian prions. *Science* **305**, 673-676
29. Post, K., Pitschke, M., Schafer, O., Wille, H., Appel, T. R., Kirsch, D., Mehlhorn, I., Serban, H., Prusiner, S. B., and Riesner, D. (1998) Rapid acquisition of beta-sheet structure in the prion protein prior to multimer formation. *Biol Chem* **379**, 1307-1317
30. Ziaunys, M., Sakalauskas, A., Mikalauskaite, K., Snieckute, R., and Smirnovas, V. (2021) Temperature-Dependent Structural Variability of Prion Protein Amyloid Fibrils. *International Journal of Molecular Sciences* **22**
31. Powers, E. T., and Powers, D. L. (2008) Mechanisms of protein fibril formation: nucleated polymerization with competing off-pathway aggregation. *Biophys J* **94**, 379-391
32. Spehar, K., Ding, T., Sun, Y., Kedia, N., Lu, J., Nahass, G. R., Lew, M. D., and Bieschke, J. (2018) Super-resolution Imaging of Amyloid Structures over Extended Times by Using Transient Binding of Single Thioflavin T Molecules. *Chembiochem* **19**, 1944-1948
33. Schmidt, C., Fizet, J., Properzi, F., Batchelor, M., Sandberg, M. K., Edgeworth, J. A., Afran, L., Ho, S., Badhan, A., Klier, S., Linehan, J. M., Brandner, S., Hosszu, L. L., Tattum, M. H., Jat, P., Clarke, A. R., Klohn, P. C., Wadsworth, J. D., Jackson, G. S., and Collinge, J. (2015) A systematic investigation of production of synthetic prions from recombinant prion protein. *Open Biol* **5**, 150165

34. Swietnicki, W., Morillas, M., Chen, S. G., Gambetti, P., and Surewicz, W. K. (2000) Aggregation and fibrillization of the recombinant human prion protein huPrP90-231. *Biochemistry* **39**, 424-431
35. Stohr, J., Weinmann, N., Wille, H., Kaimann, T., Nagel-Steger, L., Birkmann, E., Panza, G., Prusiner, S. B., Eigen, M., and Riesner, D. (2008) Mechanisms of prion protein assembly into amyloid. *Proc Natl Acad Sci U S A* **105**, 2409-2414
36. Atarashi, R., Moore, R. A., Sim, V. L., Hughson, A. G., Dorward, D. W., Onwubiko, H. A., Priola, S. A., and Caughey, B. (2007) Ultrasensitive detection of scrapie prion protein using seeded conversion of recombinant prion protein. *Nat Methods* **4**, 645-650
37. Willbold, D., Strodel, B., Schroder, G. F., Hoyer, W., and Heise, H. (2021) Amyloid-type Protein Aggregation and Prion-like Properties of Amyloids. *Chem Rev* **121**, 8285-8307
38. Cohen, S. I., Linse, S., Luheshi, L. M., Hellstrand, E., White, D. A., Rajah, L., Otzen, D. E., Vendruscolo, M., Dobson, C. M., and Knowles, T. P. (2013) Proliferation of amyloid-beta42 aggregates occurs through a secondary nucleation mechanism. *Proc Natl Acad Sci U S A* **110**, 9758-9763
39. Buell, A. K., Galvagnion, C., Gaspar, R., Sparr, E., Vendruscolo, M., Knowles, T. P., Linse, S., and Dobson, C. M. (2014) Solution conditions determine the relative importance of nucleation and growth processes in alpha-synuclein aggregation. *Proc Natl Acad Sci U S A* **111**, 7671-7676
40. Milto, K., Michailova, K., and Smirnovas, V. (2014) Elongation of Mouse Prion Protein Amyloid-Like Fibrils: Effect of Temperature and Denaturant Concentration. *Plos One* **9**
41. Jarrett, J. T., and Lansbury, P. T., Jr. (1993) Seeding "one-dimensional crystallization" of amyloid: a pathogenic mechanism in Alzheimer's disease and scrapie? *Cell* **73**, 1055-1058
42. Cohen, E., Bieschke, J., Perciavalle, R. M., Kelly, J. W., and Dillin, A. (2006) Opposing activities protect against age-onset proteotoxicity. *Science* **313**, 1604-1610
43. Terry, C., Wenborn, A., Gros, N., Sells, J., Joiner, S., Hosszu, L. L., Tattum, M. H., Panico, S., Clare, D. K., Collinge, J., Saibil, H. R., and Wadsworth, J. D. (2016) Ex vivo mammalian prions are formed of paired double helical prion protein fibrils. *Open Biol* **6**
44. Du, D., Murray, A. N., Cohen, E., Kim, H. E., Simkovsky, R., Dillin, A., and Kelly, J. W. (2011) A kinetic aggregation assay allowing selective and sensitive amyloid-beta quantification in cells and tissues. *Biochemistry* **50**, 1607-1617
45. Jain, S., and Udgaonkar, J. B. (2008) Evidence for stepwise formation of amyloid fibrils by the mouse prion protein. *J Mol Biol* **382**, 1228-1241
46. Honda, R. P., and Kuwata, K. (2017) The native state of prion protein (PrP) directly inhibits formation of PrP-amyloid fibrils in vitro. *Scientific Reports* **7**
47. Bieschke, J., Zhang, Q., Powers, E. T., Lerner, R. A., and Kelly, J. W. (2005) Oxidative metabolites accelerate Alzheimer's amyloidogenesis by a two-step mechanism, eliminating the requirement for nucleation. *Biochemistry* **44**, 4977-4983
48. Klement, K., Wieligmann, K., Meinhardt, J., Hortschansky, P., Richter, W., and Fandrich, M. (2007) Effect of different salt ions on the propensity of aggregation and on the structure of Alzheimer's abeta(1-40) amyloid fibrils. *J Mol Biol* **373**, 1321-1333
49. Hartl, F. U. (1996) Molecular chaperones in cellular protein folding. *Nature* **381**, 571-579
50. Muchowski, P. J., and Wacker, J. L. (2005) Modulation of neurodegeneration by molecular chaperones. *Nat Rev Neurosci* **6**, 11-22
51. Evans, C. G., Wisen, S., and Gestwicki, J. E. (2006) Heat shock proteins 70 and 90 inhibit early stages of amyloid beta-(1-42) aggregation in vitro. *J Biol Chem* **281**, 33182-33191
52. Wacker, J. L., Zareie, M. H., Fong, H., Sarikaya, M., and Muchowski, P. J. (2004) Hsp70 and Hsp40 attenuate formation of spherical and annular polyglutamine oligomers by partitioning monomer. *Nat Struct Mol Biol* **11**, 1215-1222
53. Rosas, P. C., Nagaraja, G. M., Kaur, P., Panossian, A., Wickman, G., Garcia, L. R., Al-Khamis, F. A., and Asea, A. A. (2016) Hsp72 (HSPA1A) Prevents Human Islet Amyloid Polypeptide

Aggregation and Toxicity: A New Approach for Type 2 Diabetes Treatment. *PLoS One* **11**, e0149409
54. Bongiovanni, M. N., Aprile, F. A., Sormanni, P., and Vendruscolo, M. (2018) A Rationally Designed Hsp70 Variant Rescues the Aggregation-Associated Toxicity of Human IAPP in Cultured Pancreatic Islet beta-Cells. *Int J Mol Sci* **19**
55. Fernandez-Funez, P., Sanchez-Garcia, J., de Mena, L., Zhang, Y., Levites, Y., Khare, S., Golde, T. E., and Rincon-Limas, D. E. (2016) Holdase activity of secreted Hsp70 masks amyloid-beta42 neurotoxicity in Drosophila. *Proc Natl Acad Sci U S A* **113**, E5212-5221
56. Bieschke, J., Russ, J., Friedrich, R. P., Ehrnhoefer, D. E., Wobst, H., Neugebauer, K., and Wanker, E. E. (2010) EGCG remodels mature alpha-synuclein and amyloid-beta fibrils and reduces cellular toxicity. *Proc Natl Acad Sci U S A* **107**, 7710-7715
57. Ehrnhoefer, D. E., Bieschke, J., Boeddrich, A., Herbst, M., Masino, L., Lurz, R., Engemann, S., Pastore, A., and Wanker, E. E. (2008) EGCG redirects amyloidogenic polypeptides into unstructured, off-pathway oligomers. *Nat Struct Mol Biol* **15**, 558-566
58. Bieschke, J., Herbst, M., Wiglenda, T., Friedrich, R. P., Boeddrich, A., Schiele, F., Kleckers, D., Lopez del Amo, J. M., Gruning, B. A., Wang, Q., Schmidt, M. R., Lurz, R., Anwyl, R., Schnoegl, S., Fandrich, M., Frank, R. F., Reif, B., Gunther, S., Walsh, D. M., and Wanker, E. E. (2012) Small-molecule conversion of toxic oligomers to nontoxic beta-sheet-rich amyloid fibrils. *Nat Chem Biol* **8**, 93-101
59. Lam, H. T., Graber, M. C., Gentry, K. A., and Bieschke, J. (2016) Stabilization of alpha-Synuclein Fibril Clusters Prevents Fragmentation and Reduces Seeding Activity and Toxicity. *Biochemistry* **55**, 675-685
60. Cohen, S. I., Arosio, P., Presto, J., Kurudenkandy, F. R., Biverstal, H., Dolfe, L., Dunning, C., Yang, X., Frohm, B., Vendruscolo, M., Johansson, J., Dobson, C. M., Fisahn, A., Knowles, T. P., and Linse, S. (2015) A molecular chaperone breaks the catalytic cycle that generates toxic Abeta oligomers. *Nat Struct Mol Biol* **22**, 207-213
61. Amin, L., and Harris, D. A. (2021) Abeta receptors specifically recognize molecular features displayed by fibril ends and neurotoxic oligomers. *Nat Commun* **12**, 3451
62. Bove-Fenderson, E., Urano, R., Straub, J. E., and Harris, D. A. (2017) Cellular prion protein targets amyloid-beta fibril ends via its C-terminal domain to prevent elongation. *J Biol Chem* **292**, 16858-16871
63. Freir, D. B., Nicoll, A. J., Klyubin, I., Panico, S., Mc Donald, J. M., Risse, E., Asante, E. A., Farrow, M. A., Sessions, R. B., Saibil, H. R., Clarke, A. R., Rowan, M. J., Walsh, D. M., and Collinge, J. (2011) Interaction between prion protein and toxic amyloid beta assemblies can be therapeutically targeted at multiple sites. *Nat Commun* **2**, 336
64. Nicoll, A. J., Panico, S., Freir, D. B., Wright, D., Terry, C., Risse, E., Herron, C. E., O'Malley, T., Wadsworth, J. D., Farrow, M. A., Walsh, D. M., Saibil, H. R., and Collinge, J. (2013) Amyloid-beta nanotubes are associated with prion protein-dependent synaptotoxicity. *Nat Commun* **4**, 2416
65. Grassmann, A., Wolf, H., Hofmann, J., Graham, J., and Vorberg, I. (2013) Cellular aspects of prion replication in vitro. *Viruses* **5**, 374-405
66. Choudhury, A., Marks, D. L., Proctor, K. M., Gould, G. W., and Pagano, R. E. (2006) Regulation of caveolar endocytosis by syntaxin 6-dependent delivery of membrane components to the cell surface. *Nat Cell Biol* **8**, 317-328
67. Hegde, R. S., Mastrianni, J. A., Scott, M. R., DeFea, K. A., Tremblay, P., Torchia, M., DeArmond, S. J., Prusiner, S. B., and Lingappa, V. R. (1998) A transmembrane form of the prion protein in neurodegenerative disease. *Science* **279**, 827-834
68. Stewart, R. S., and Harris, D. A. (2005) A transmembrane form of the prion protein is localized in the Golgi apparatus of neurons. *J Biol Chem* **280**, 15855-15864
69. Shi, Z., Sachs, J. N., Rhoades, E., and Baumgart, T. (2015) Biophysics of alpha-synuclein induced membrane remodelling. *Phys Chem Chem Phys* **17**, 15561-15568

70. Lashuel, H. A., Hartley, D., Petre, B. M., Walz, T., and Lansbury, P. T., Jr. (2002) Neurodegenerative disease: amyloid pores from pathogenic mutations. *Nature* **418**, 291
71. Jin, S., Kedia, N., Illes-Toth, E., Haralampiev, I., Prisner, S., Herrmann, A., Wanker, E. E., and Bieschke, J. (2016) Amyloid-beta(1-42) Aggregation Initiates Its Cellular Uptake and Cytotoxicity. *J Biol Chem* **291**, 19590-19606
72. Friedrich, R. P., Tepper, K., Ronicke, R., Soom, M., Westermann, M., Reymann, K., Kaether, C., and Fandrich, M. (2010) Mechanism of amyloid plaque formation suggests an intracellular basis of Abeta pathogenicity. *Proc Natl Acad Sci U S A* **107**, 1942-1947
73. Hosszu, L. L., Wells, M. A., Jackson, G. S., Jones, S., Batchelor, M., Clarke, A. R., Craven, C. J., Waltho, J. P., and Collinge, J. (2005) Definable equilibrium states in the folding of human prion protein. *Biochemistry* **44**, 16649-16657
74. Jackson, G. S., Hill, A. F., Joseph, C., Hosszu, L., Power, A., Waltho, J. P., Clarke, A. R., and Collinge, J. (1999) Multiple folding pathways for heterologously expressed human prion protein. *Biochim Biophys Acta* **1431**, 1-13
75. Sun, Y. (2022) Direct Observation of Prion Protein Fibril Elongation Kinetics Reveals Competing Fibril Populations with Distinct Structural and Dynamic Properties. *BioRxiv*

Figure 1

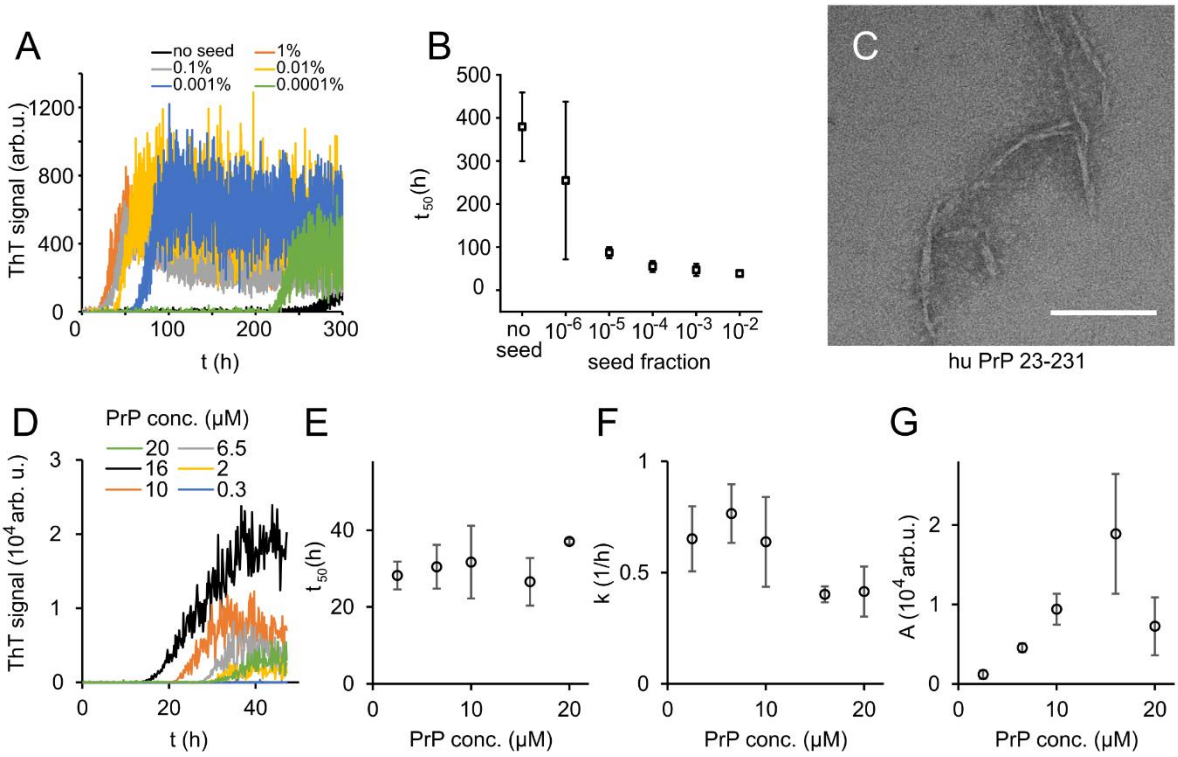

Figure 1: Native aggregation assay (NAA) of human PrP (23-231). (A) Seed titration experiment using seed generated from hPrP (23-231) fibrils formed de novo in NAA, seed fraction (w/w), 2.5 µM PrP, pH 6.8, 42°C. (B) Plot of lag phase vs. fraction of seed, n=3. (C) TEM image of hPrP (23-231) fibrils formed after 166h incubation. (D-G) Titration of PrP concentration (0.3µM-20µM) in ThT aggregation assays containing 0.01% seed, pH 6.8, 42°C. (D) Plot of ThT fluorescence vs. time. (E) Plot of lag time t_{50} vs. PrP concentration. (F) Plot of fluorescence amplitude *A* vs. PrP concentration. (G) Plot of elongation rate constant *k* vs. PrP concentration.

Figure 2

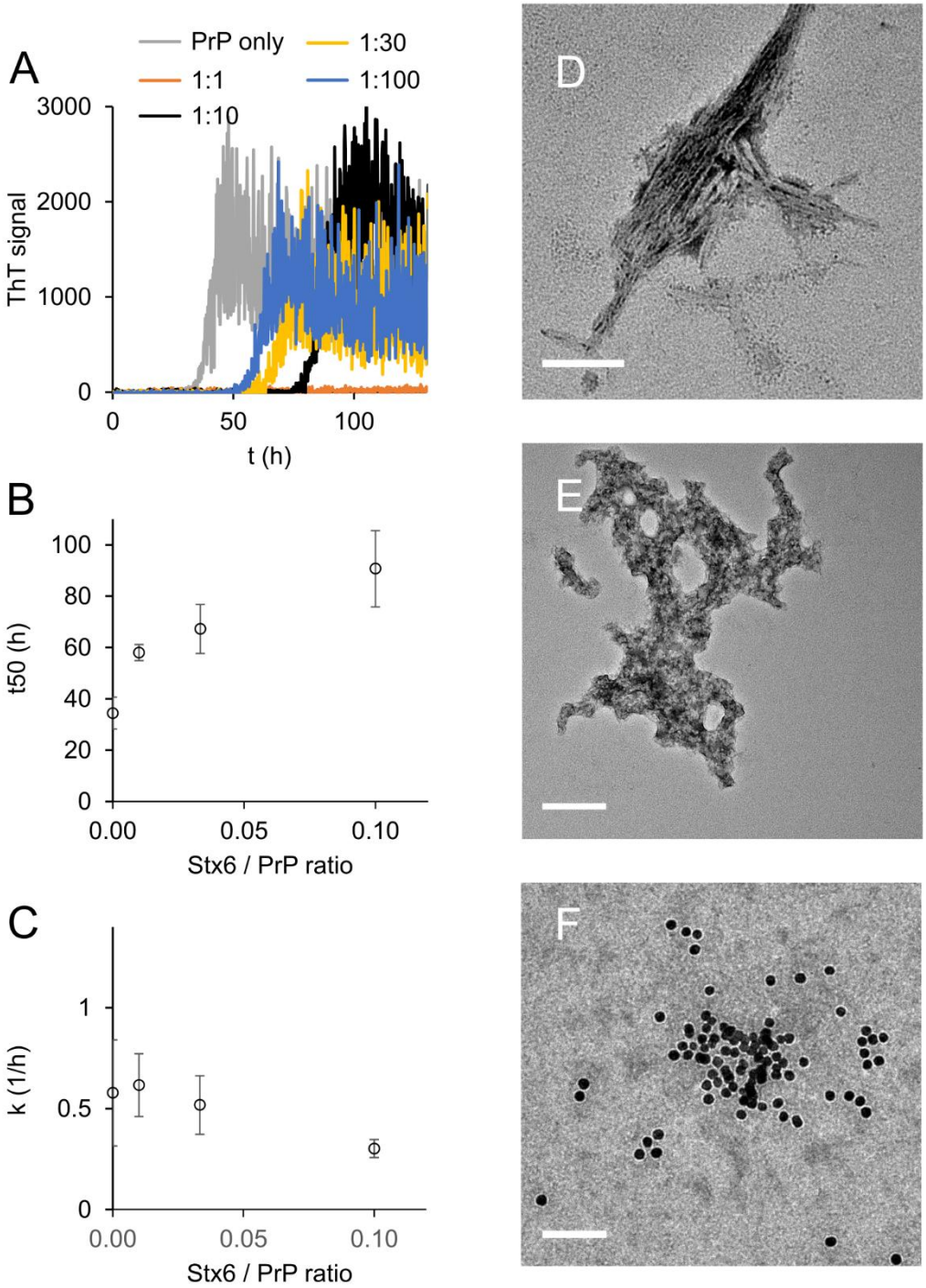

Figure 2: Syntaxin 6 delays hPrP 23 fibril formation at molar ratios of 1:1 – 1:100; 2.5 µM PrP, pH 6.8, 42°C, 0.01% seed. (A) ThT fluorescence vs time. (B) Plot of lag phase t_{50} vs. molar ratio of stx6 / PrP, n=3. (C) Plot of elongation rate constant *k* vs. molar ratio of stx6 / PrP. (D) TEM image of a cluster of hPrP (23-231) fibrils at assay endpoint without STX6. (E) TEM image of hPrP (23-231) co-aggregated with stx6 at 1:10 (stx6 / PrP) molar ratio under standard NAA conditions for 65h. (F) Immuno-TEM image of hPrP (23-231) – stx6 co-aggregate cluster. Stx6 is immunogold labelled with (STX6 Rabbit Polyclonal Primary Ab); scale bars 200 nm.

Figure 3

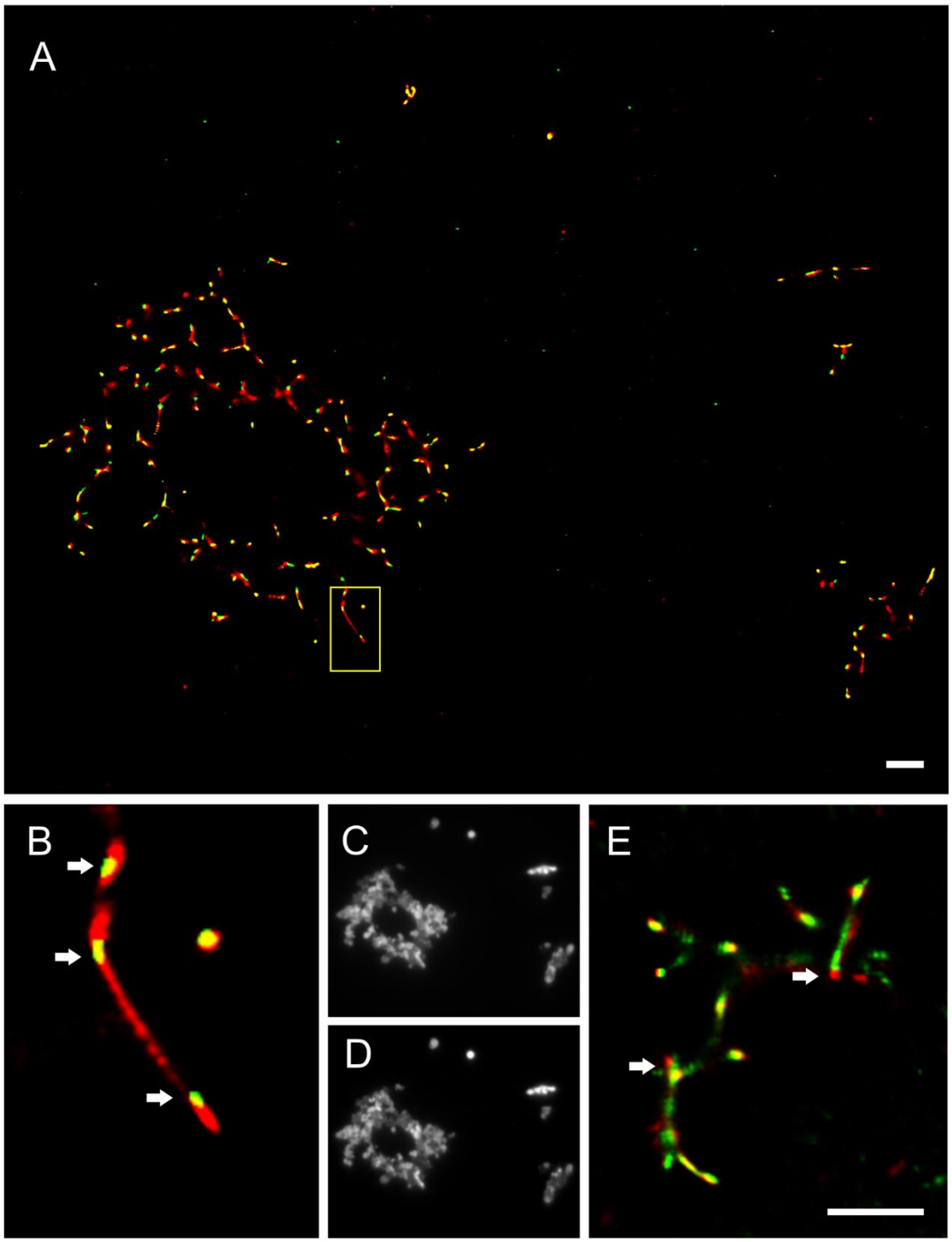

Figure 3: Super resolution image of hPrP23 fibrils incubated with stx6. PrP (2.5 µM) was pre-aggregated in NAA for 115h, and incubated with stx6 for 1h. hPrP was Yvisualized by TAB imaging using 10 nM Nile red dye; stx6 was labelled with AlexaFluor488 (A-D) or AlexaFluor647 (E) and imaged by dSTORM. (A) SR image overlay shows stx6 binding at hotspots and PrP fibril ends. (B) Magnified area from (A). (C) Widefield image taken with green laser (561nm) illumination. (D) Widefield image taken under blue laser (473nm) illumination. (E) SR image overlay of PrP and STX6-AlexaFluor647 images; scale bars 2 µm.

Figure 4

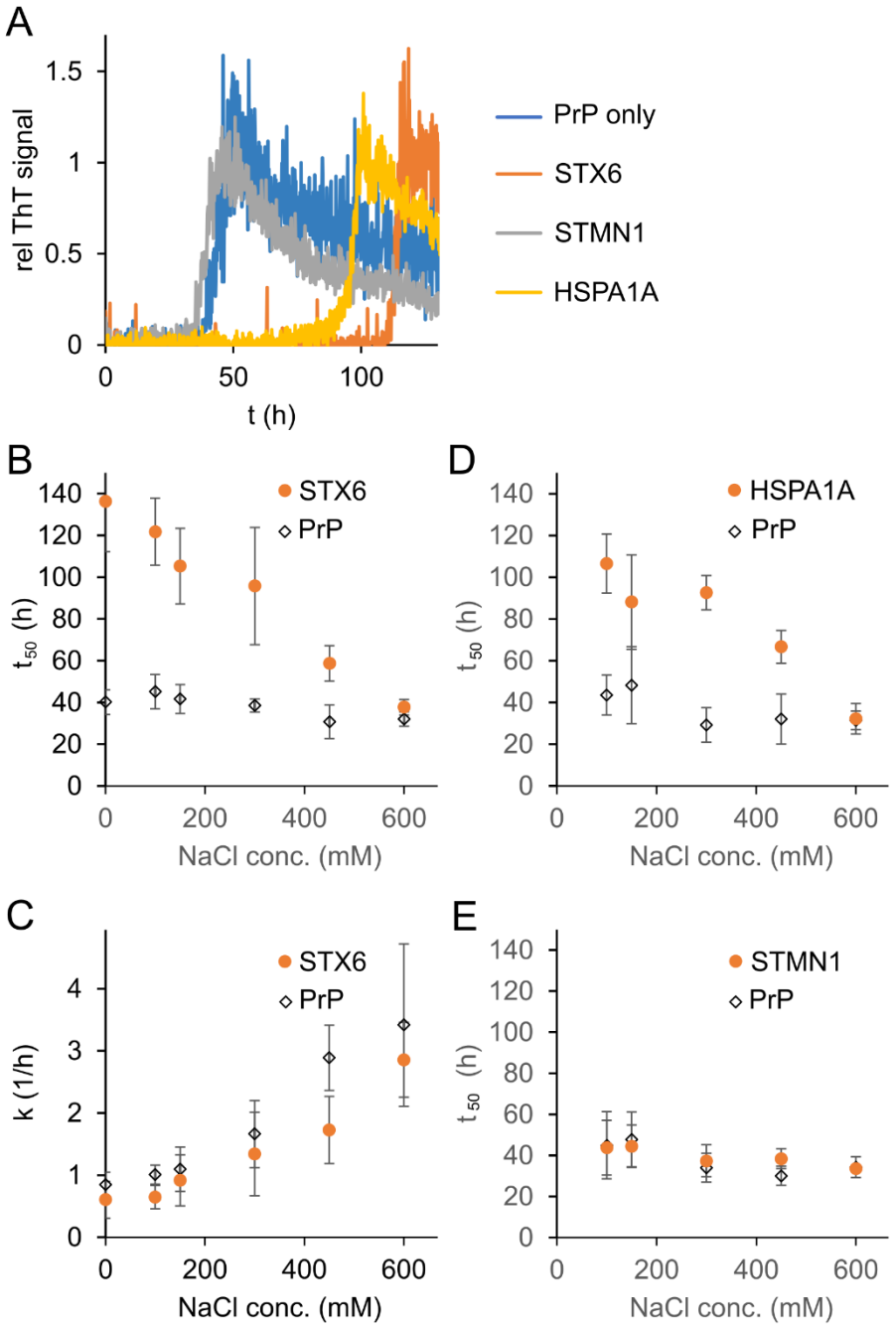

Figure 4: Salt-dependent inhibition of fibril formation. Syntaxin 6, Stathmin1, HSPA1A 1:10 molar ratio were incubated with hPrP23. (A) Plot of relative ThT fluorescence profiles vs time in NAA (150 mM NaCl, 42°C, 0.01% seed,). (B) Plot of lag phase t_{50} vs NaCl concentration for hPrP23 alone vs co-aggregated with syntaxin 6 (STX6) at 1:10 molar ratio. (C) Plot of elongation rate constant *k* vs. NaCl concentration. (D) Plot of lag phase t_{50} vs NaCl concentration for hPrP 23-231 alone vs co-aggregated with HSPA1A at 1:10 molar ratio. (E) Plot of lag phase t_{50} vs NaCl concentration for hPrP 23-231 alone vs co-aggregated with stathmin 1 (STMN1) at 1:10 molar ratio.

Figure 5

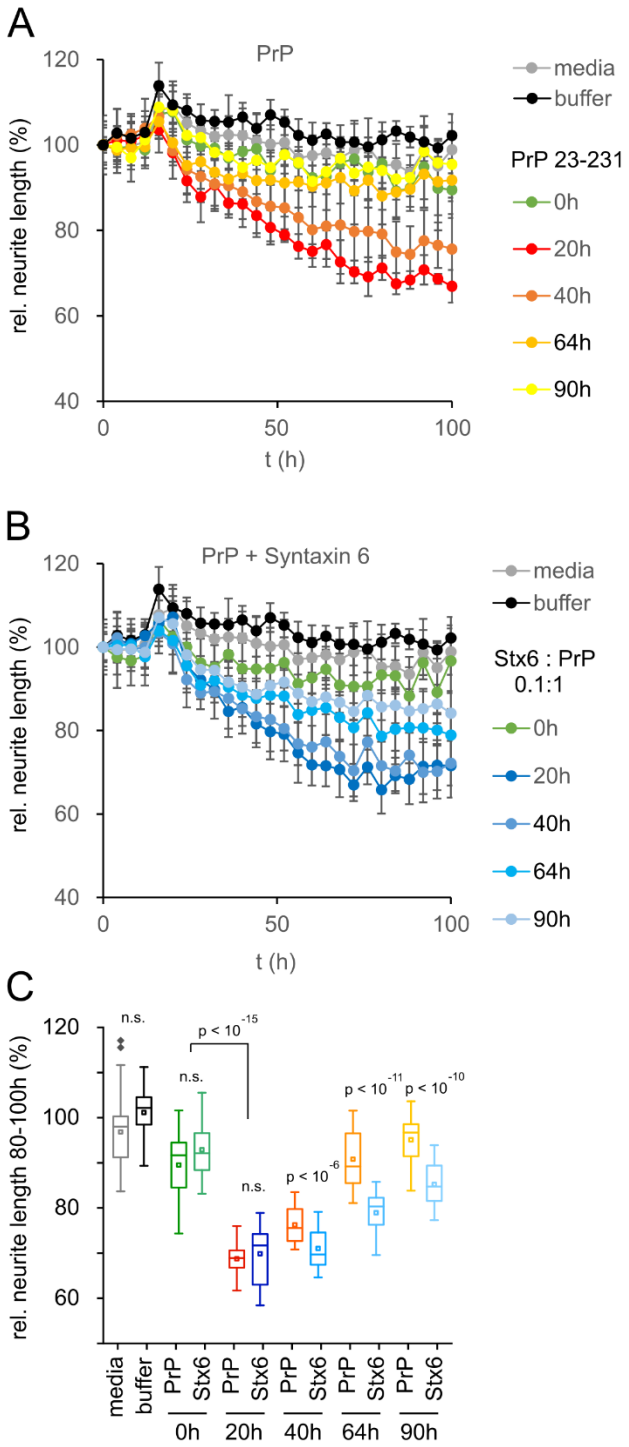

Figure 5: Toxicity in mouse primary neurons incubated with hPrP23 / stx6 at different aggregation time points. NAA was performed as in Figure 2 and samples were diluted 1:10 into cell culture media at the indicated time points (0h, 20h, 40h, 64h, 90h). (A) Plot of effect of PrP (250 nM) on neurite length compared to effect of media or NAA assay buffer at the same dilution, n=6. (B) Plot of effect of hPrP 23-231 co-aggregated with stx6 (1:10 molar ratio). (C) Box plot of average relative neurite lengths between 80-100h incubation of PrP in the cell culture media. P-values are derived from ANOVA testing between PrP vs PrP/stx6 samples at each time point.

Figure S1

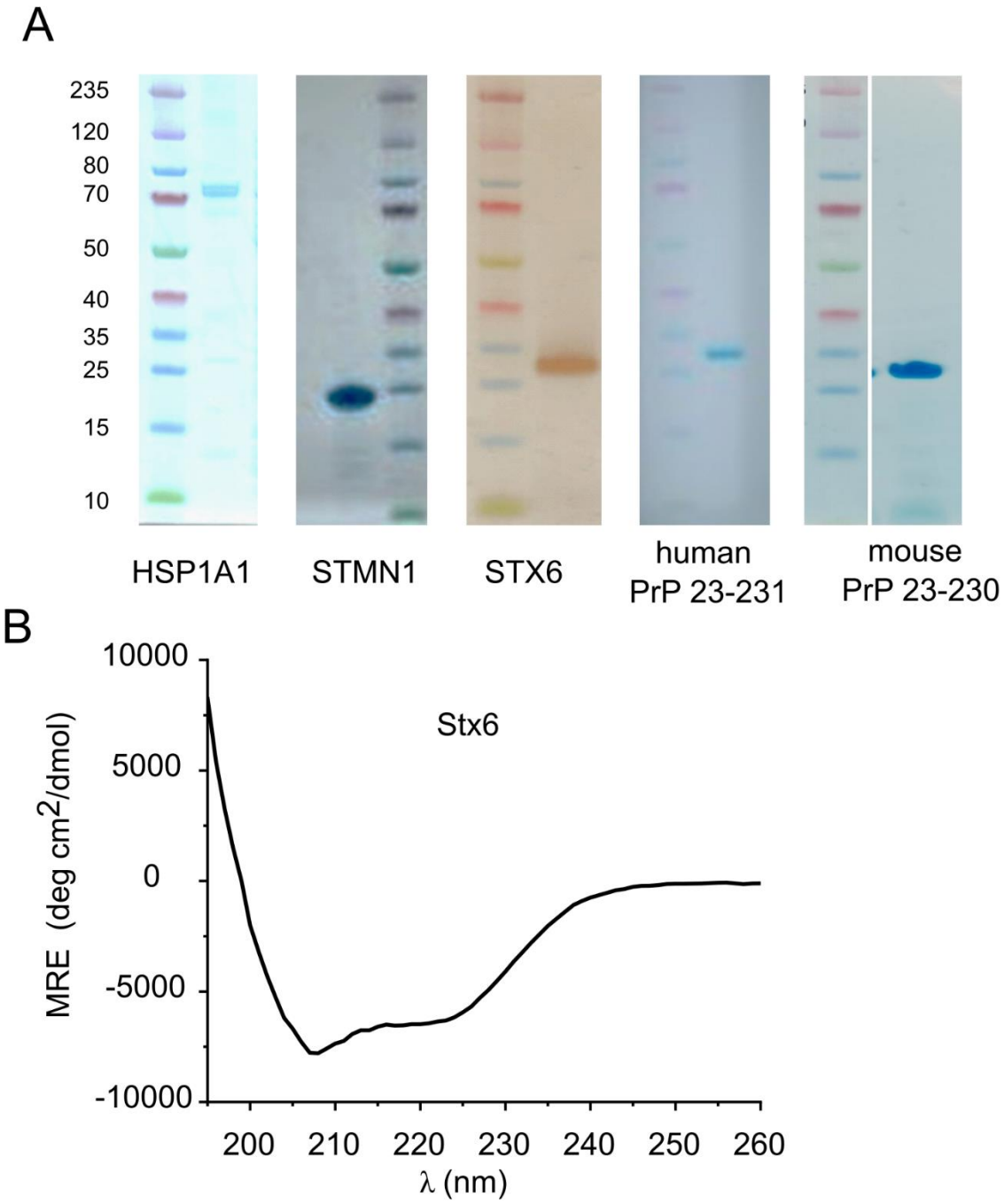

Supplementary Figure S1. (A) Coomassie/Silver stained gels of purified hPrP23, mPrP23 and candidate proteins. (B) Circular dichroism spectrum of purified syntaxin 6 protein showing a mostly alpha helical shape with minima at 208nm and 223nm.

Figure S2

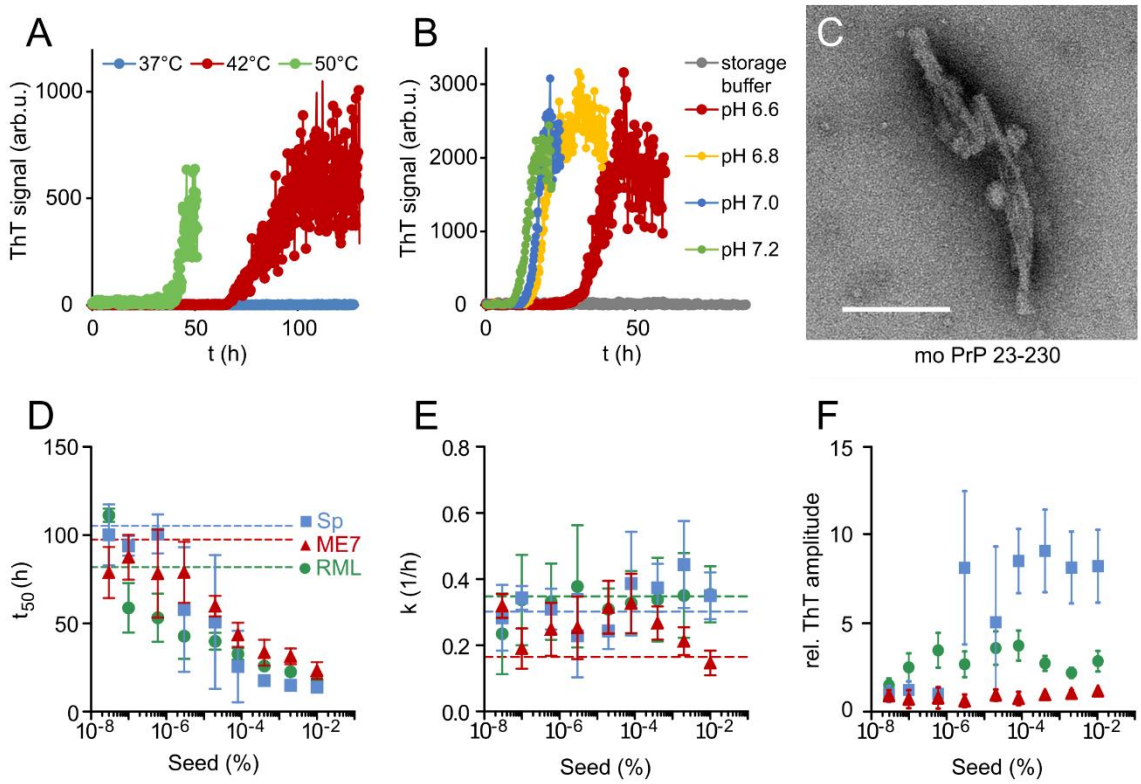

Supplementary Figure S2: Optimisation of NAA on mouse PrP23. (A) Plot of ThT fluorescence over time at 37°C, 42°C and 50°C (pH 7.4). (B) NAA aggregation kinetics at pH 6.6, 6.8, 7.0 and 7.2 at 42°C. (C) TEM image of mPrP23 fibrils formed after 47h incubation at pH 6.8, 42°C; scale bar 100 nm. (D-F) Seed titration experiments comparing seeding from synthetic PrP fibrils (Sp) and purified prion rods from mouse prion strains ME7 and RML. (D) Plot of time to half-maximal fluorescence (t_{50}) (E) elongation rate constant (k), and (F) ThT amplitudes as functions of seed concentration, n=5.

Figure S3

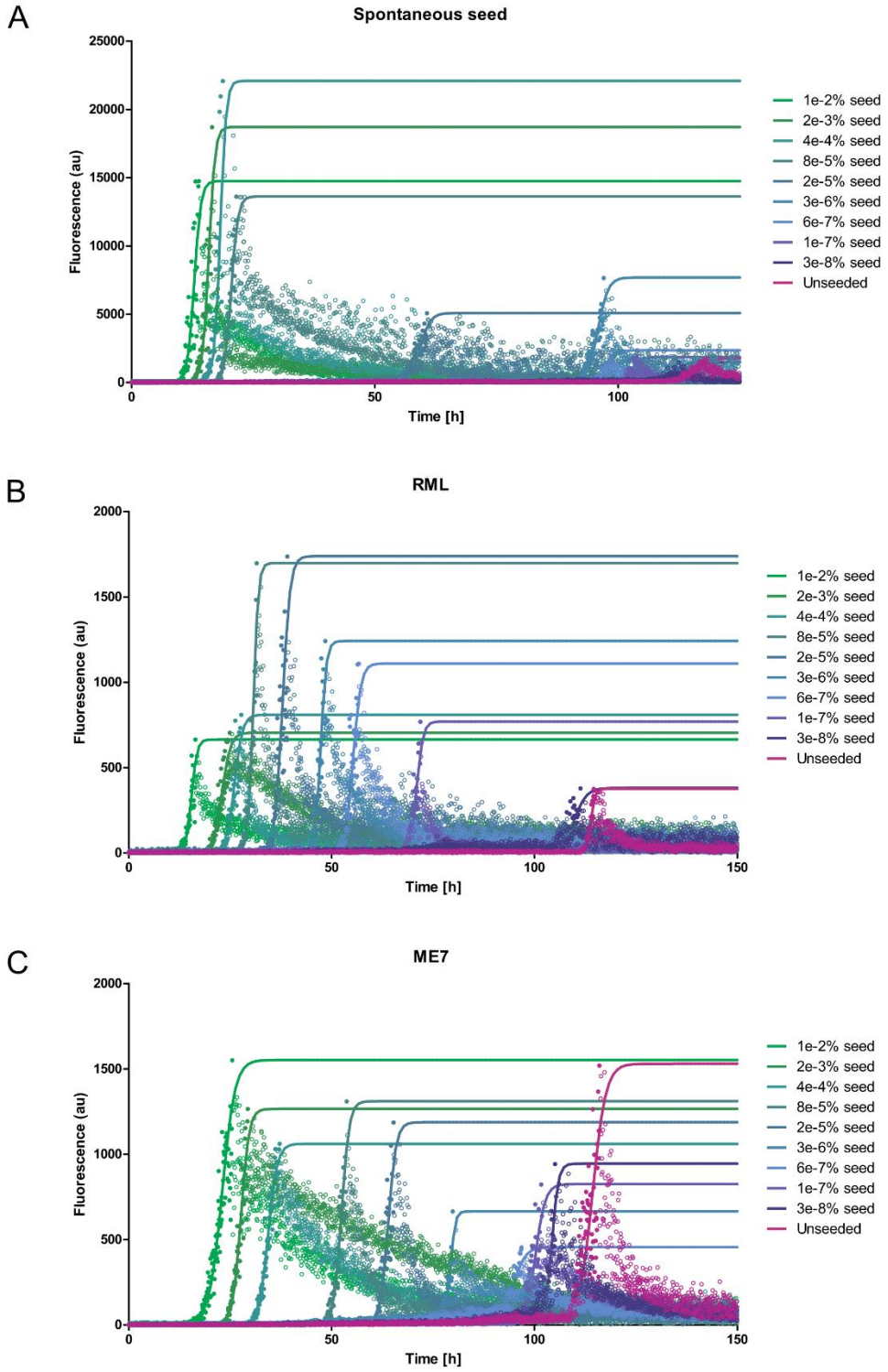

Supplementary Figure S3. Graphs of NAA on mPrP23 seed titration experiments demonstrate seed concentration-dependent acceleration of fibril formation. (A) First generation (spontaneous) seed. (B) Seed generated from RML mouse strain (C) Seed generated from ME7 mouse strain.

Figure S4

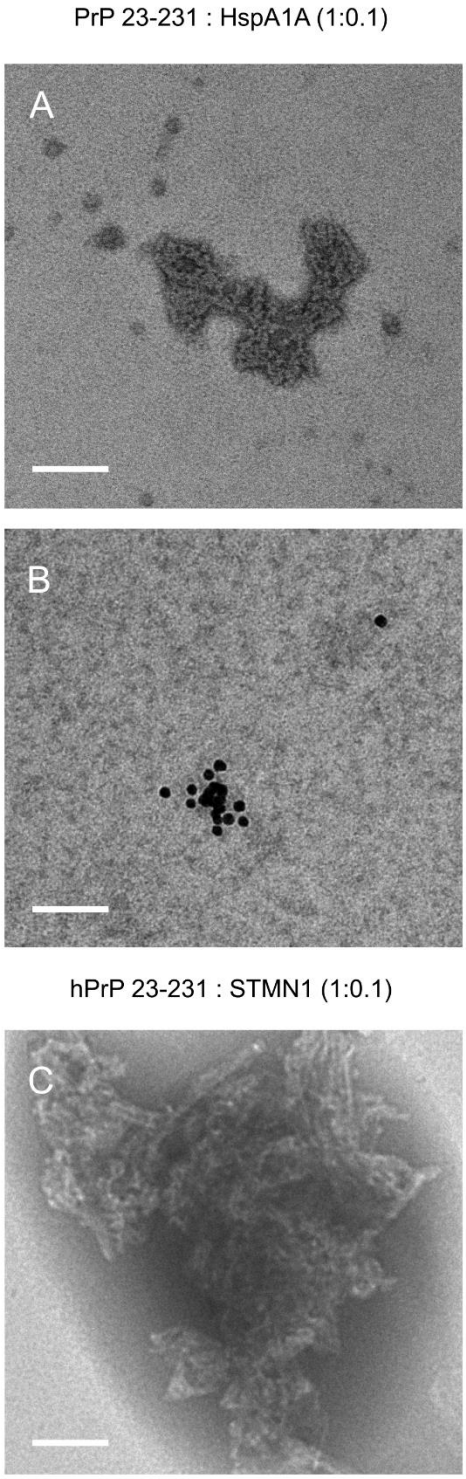

Supplementary Figure S4. TEM images of NAA aggregation end-points of hPrP23 co-aggregated with Hspa1a; A, B) or stathmin 1 (Stmn1) (C) at 1:10 molar ratio. (A) PrP forms amorphous aggregates in presence of Hspa1a. (B) Immuno-TEM of PrP / Hspa1a co-aggregation (Hsp70 Rabbit Polyclonal primary Ab, goat anti-Rabbit IgG conjugated to 10nm colloidal gold particles). (C) PrP forms fibrillar aggregates in presence of Stmn1.

Figure S5

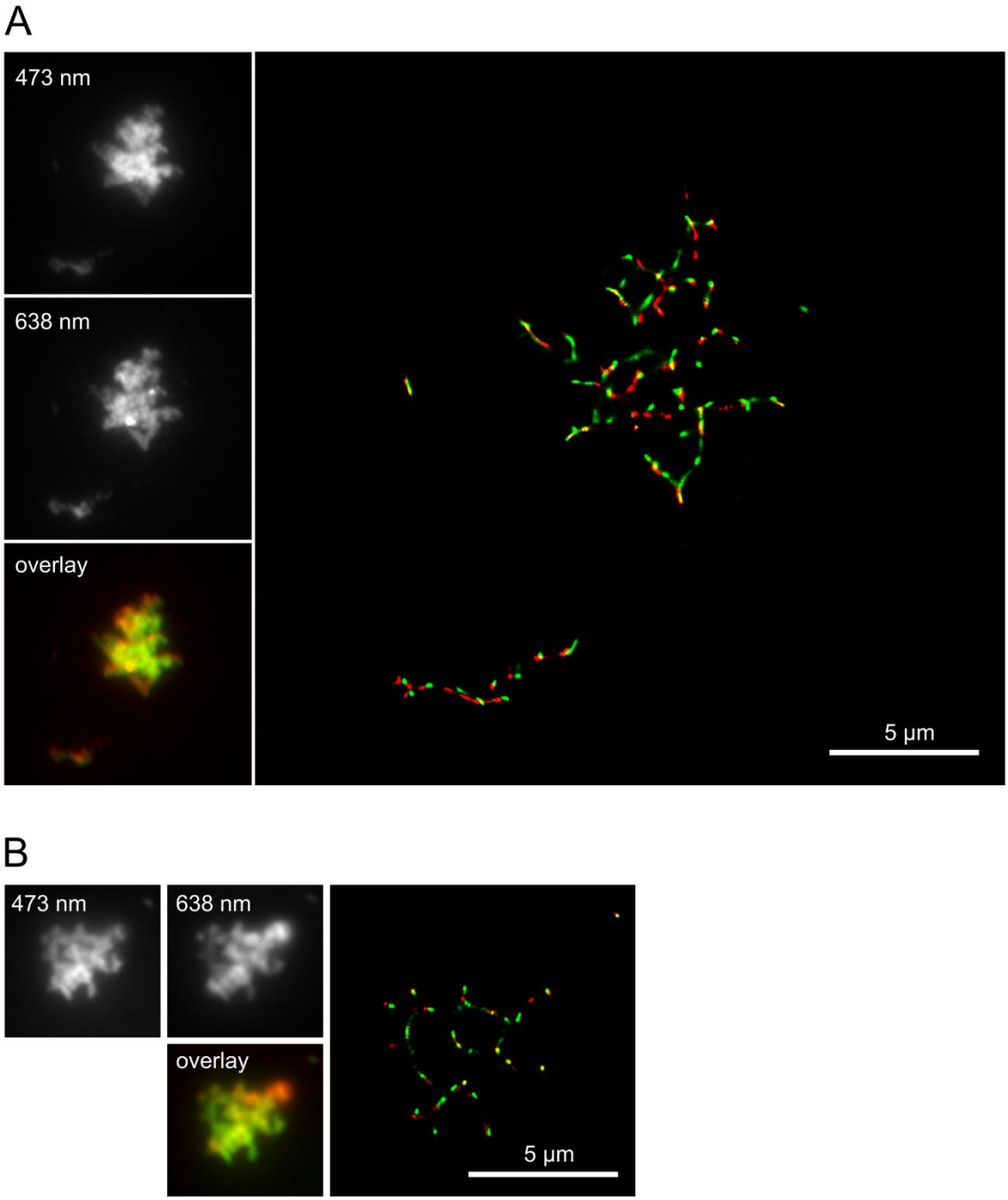

Supplementary Figure S5. Overlay of dSTORM SR images taken at 473 nm and 638 nm excitation. Co-aggregates of hPrP23 and stx6 formed in NAA under conditions of Figure 3. (A) Co-aggregation of hPrP23 labelled with AlexaFluor 647-NHS (2.5 µM, 3% labelled, 95% unlabelled) with 10 nM Stx6 labelled with AlexaFluor488-NHS (B) Co-aggregation of PrP labelled with AlexaFluor 647-NHS (2.5 µM, 5% labelled, 95% unlabelled) with stx6 at 1:10 molar ratio (Stx6, 250 nM, 4% labelled, 96% unlabelled). *Insets*: wide field images with 473 nm and 638 nm excitation and composite image of both channels.

Figure S6

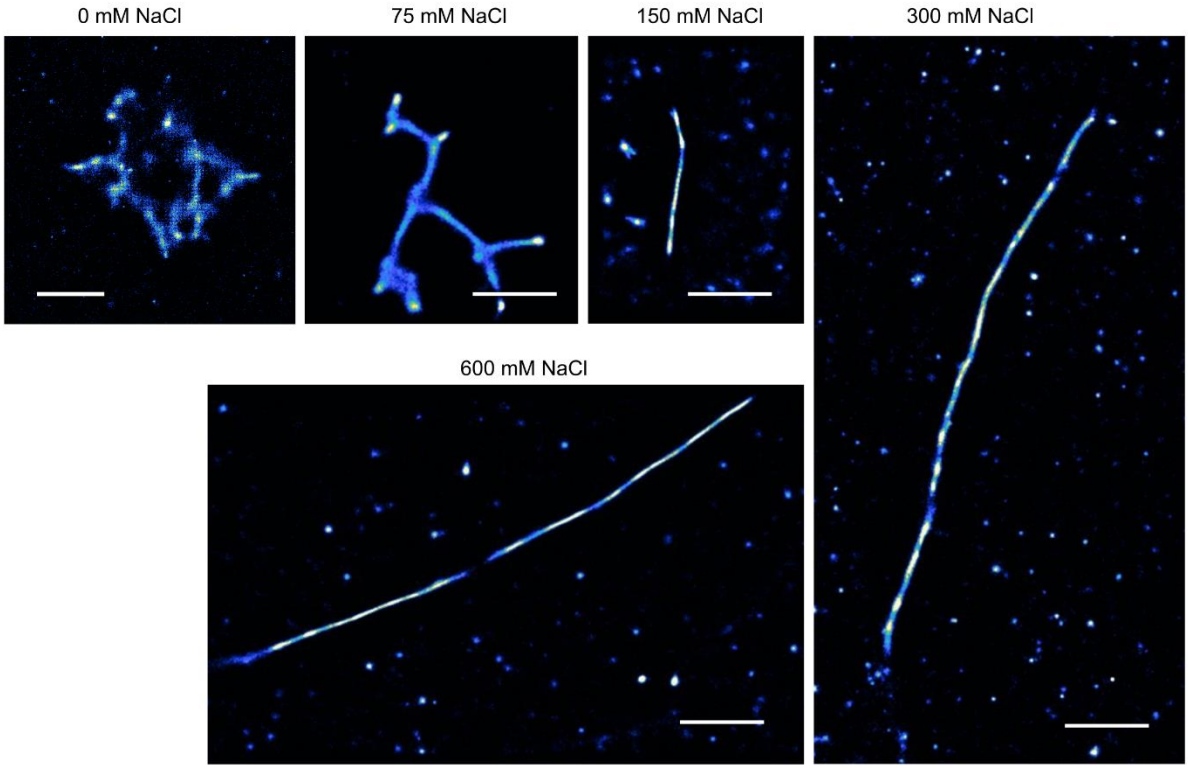

Supplementary Figure S6. TAB SR microscopy images of aggregation endpoints of hPrP23 in NAA with increasing salt concentrations from 0mM to 600mM NaCl.

Figure S7

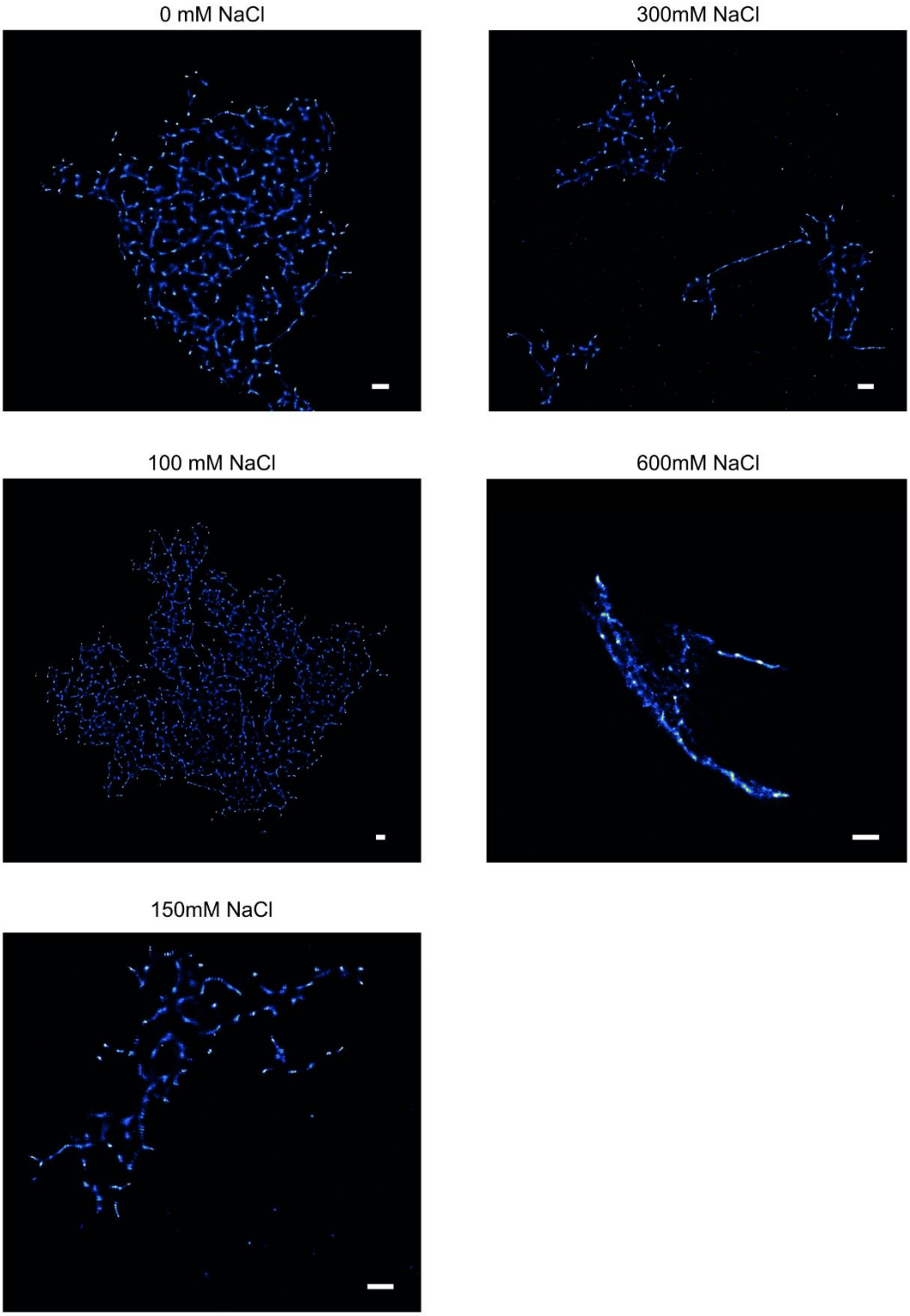

Supplementary Figure S7. TAB SR microscopy images of aggregation endpoints of hPrP23 co-aggregated with STX6 in NAA at increasing salt concentrations from 0mM to 600mM NaCl.